Added mass estimation for a pivoted cylinder undergoing vortex induced vibrations

K. Figueroa[a] and J. C. Cajas[b]

[a]*LIPC instituto de ingeniería, Universidad Nacional Autónoma de México.*
e-mail: kfigueroap@lipc.unam.mx
[b]*ENES unidad Mérida, Universidad Nacional Autónoma de México.*
e-mail: carlos.cajas@enesmerida.unam.mx

Received 23 February 2025; accepted 1 April 2025

In the present article, we propose and solve an inverse problem to estimate hydrodynamic parameters relevant to the vortex induced vibrations of a pivoted cylinder in laminar flow. For the analysis, we utilized published results from high-performance simulations of this scenario. The study focuses on estimating the added mass parameter, which is crucial in the design of fluid-structure interaction devices and certain numerical techniques for general fluid-structure interaction solvers. We obtain a quadratic relationship between the added mass parameter and the angular acceleration of the cylinder. Moreover, not only are the results significant, but the methodology employed in this article is adaptable to other numerical or experimental fluid-structure interaction results and can assist in determining important design parameters for fluid-structure interaction devices.

Keywords: Inverse problems; added mass parameter; forced-damped oscillator.

DOI: https://doi.org/10.31349/RevMexFis.72.020603

1. Introduction

Fluid structure interaction (FSI) is a complex phenomenon that combines the governing equations of fluid mechanics with those of solid mechanics. It presents challenging mathematical problems and has attracted significant attention due to its physical richness and diverse applications. Examples of FSI can be found in Refs. [13,14,16].

A specific type of FSI problem is the vortex induced vibration (VIV) of bodies immersed in fluid flow. This phenomenon occurs when the vortex shedding frequency of bluff bodies in a flow approaches the natural frequency of the structure, leading to oscillations caused by fluctuating hydrodynamic forces.

FSI has been extensively studied over the decades, with excellent references on the general theoretical framework including [1,2,15,18,19]. In particular, the VIV of circular cylinders in different configurations has been examined both experimentally [9,10,19] and numerically [3,8,11]. These studies reveal the existence of distinct response 'branches' characterized by variations in amplitude and frequency based on the system's physical parameters. For example, recent studies involving pivoted circular cylinders can be found in Ref. [5,6].

A widely used numerical strategy for solving FSI problems is the partitioned approach, where the fluid and structure solvers are executed separately and coupled iteratively. This method allows the use of pre-existing fluid and structure programs, which makes it very attractive in the field of high performance computing (HPC). An example of the implementation of the partitioned approach in the HPC framework, with some examples of applications can be found in Refs. [4], and an application of this approach to study the human heart with a partitioned multicode numerical scheme is presented in Ref. [17].

The general theoretical framework of the partitioned solution scheme and the main difficulties in both theoretical and practical aspects have been widely studied; for example, [20,21]. One of the most challenging problems is the existence of the added mass effect, which occurs in incompressible flow and is influenced by the densities of the fluid and solid, potentially leading to unstable partitioned numerical schemes as noted by [22,23]. This effect becomes critical when the densities of the fluid and the solid are similar. To treat this instability, different mathematical techniques have been utilized. Some are based on static or dynamic relaxation factors, such as the Aitken relaxation factor, [7] or the interface 'Quasi-Newton' methods, [12]. However, the most challenging cases of interest require a large number of coupling iterations or the use of extremely small relaxation factors. In both cases, the resulting computational scheme is suboptimal.

In the present article, an in-depth analysis of a particular case of VIV involving a pivoted cylinder is conducted to explore the relations of relevant parameters, such as the added mass parameter and the magnitude of the hydrodynamic forces, with the displacement of the structure. The insights gained from this canonical case can assist in developing general solution algorithms for FSI problems where the influence of added mass is significant. Based on the published results of numerical simulations from [5], an inverse problem is posed to estimate the added mass parameter, resulting in a function that relates the added mass with the cylinder's acceleration. Also, it is noteworthy that the pre-

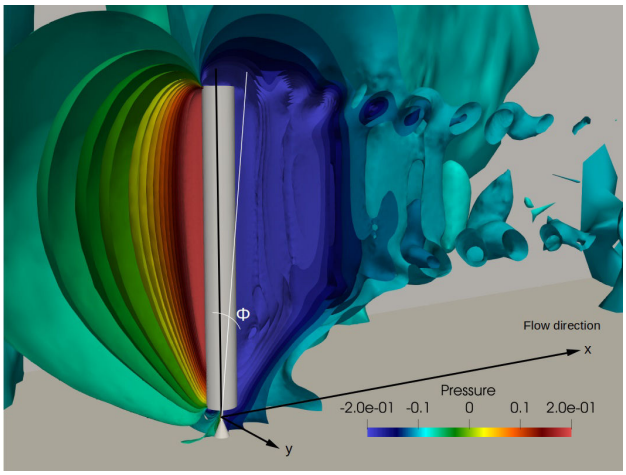

FIGURE 1. Pivoted cylinder in a fluid flow with contours of constant pressure studied in Ref. [5]. The angle Φ is measured from the vertical axis in the transverse direction of the flow.

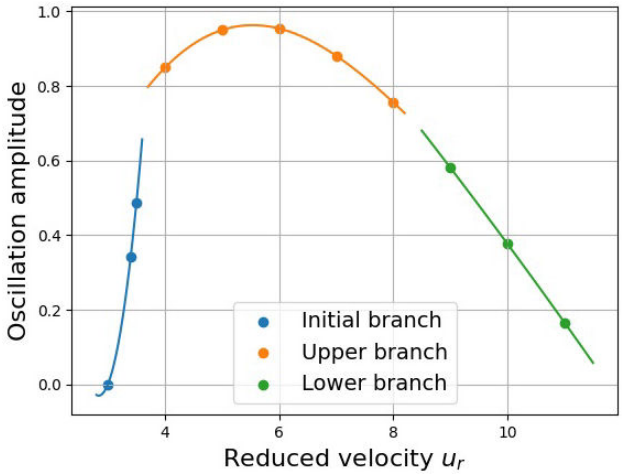

FIGURE 2. Amplitude of oscillation as a function of the reduced velocity from [5].

sented methodology can be easily extended to use other FSI numerical or experimental results.

2. Problem statement

The VIV of a pivoted finite height circular cylinder of aspect ratio (length/diameter) $AR = 10$ for laminar flow was investigated in Ref. [5]. It was demonstrated that in the regime of small amplitude oscillations, the classical forced damped oscillator equation is a valid model for the movement of the cylinder in the direction perpendicular to the current, that is

$$\ddot{\Phi} + \beta_y \dot{\Phi} + \left(\frac{2\pi}{u_r}\right)^2 \Phi \equiv \tilde{F}_y, \tag{1}$$

where Φ is the oscillation angle, β_y is the damping parameter, and $2\pi/u_r = \omega_0$ is the non-dimensional natural angular frequency of the movable structure. In the context of VIV, the use of the reduced velocity u_r is widely adopted, so the results will be presented in terms of u_r in this work. $\tilde{F}_y$ is the force exerted on the structure by the surrounding fluid, which induces the VIV.

The oscillation amplitude obtained in the same reference in the transverse direction as a function of u_r is illustrated in Fig. 2. Three response branches are identified: the initial branch, where the VIV starts and relatively small oscillation amplitudes are obtained; the upper branch, where the maximum oscillation amplitudes are observed; and the lower branch, where the amplitude of oscillations diminishes before desynchronization occurs.

Considering that the value of the added mass parameter is generally difficult to obtain and is unknown for this case, we propose using inverse parameter identification problems to obtain this value along with other relevant physical quantities using the published results of [5]. To make possible the estimation of the added mass parameter, it is proposed to decompose the hydrodynamic force as $\tilde{F}_y$ into different contributions: one proportional to the angular acceleration via the added mass coefficient m_a, another proportional to the angular velocity through a drag coefficient c_d, an oscillatory term that drives the movement of the structure with amplitudes A_y and B_y, and a constant term C_y,

$$\tilde{F}_y = -m_a\ddot{\Phi} - c_d\dot{\Phi} + A_y \sin(\omega_y t) + B_y \cos(\omega_y t) + C_y,$$

with this decomposition, the following equation is obtained

$$\ddot{\Phi}(1+m_a) + \dot{\Phi}(\beta + c_d) + \left(\frac{2\pi}{u_r}\right)^2 \Phi = A_y \sin(\omega_y t) + B_y \cos(\omega_y t) + C_y, \tag{2}$$

where ω_y is the oscillation frequency of the hydrodynamic force acting on the structure, which is close to the natural frequency $2\pi/u_r = \omega_0$ when synchronization is obtained. Note that the signs of the added mass contribution and the drag contribution are chosen to oppose the movement of the structure. Furthermore, it should be emphasized that Eq. (2) is not restricted to laminar cases and can also be applied to turbulent scenarios, as long as the requisite number of forcing frequencies relevant to the case under consideration are included in the decomposition.

Equation (2), can be integrated twice in the interval (t_0, t) to pose an inverse problem, obtaining

$$\Phi(t) - \Phi_0 - \dot{\Phi}_0(t-t_0) + \frac{\beta + c_d}{1+m_a} \times [F(t) - \Phi_0(t-t_0)] + \frac{[2\pi/u_r]^2}{1+m_a}\int_{t_0}^{t} F(s)ds = \frac{A_y}{1+m_a}\int_{t_0}^{t} I(s)ds + \frac{B_y}{1+m_a}\int_{t_0}^{t} J(s)ds + \frac{C_y}{1+m_a}\left(\frac{t^2-t_0^2}{2} - t_0(t-t_0)\right), \tag{3}$$

where

$$\Phi_0 = \Phi(t_0),\ \dot{\Phi}_0 = \dot{\Phi}(t_0),$$
$$F(t) = \int_{t_0}^{t} \Phi(s)ds, \quad I(t) = \int_{t_0}^{t} \sin(\omega_y s)ds,$$
$$J(t) = \int_{t_0}^{t} \cos(\omega_y s)ds,$$

in order to simplify Eq. (3) the following parameters and functions are defined

$$a = \frac{\beta + c_d}{1+m_a}, \quad b = \frac{[2\pi/u_r]^2}{1+m_a}, \quad c = \frac{A_y}{1+m_a},$$
$$d = \frac{B_y}{1+m_a}, \quad e = \frac{C_y}{1+m_a},$$
$$C_1(t) = F(t) - \Phi_0(t-t_0),$$
$$C_2(t) = \int_{t_0}^{t} F(s)ds, \quad C_3(t) = \int_{t_0}^{t} I(s)ds,$$
$$C_4(t) = \int_{t_0}^{t} J(s)ds, \quad C_5(t) = \frac{t^2 - t_0^2}{2} - t_0(t-t_0).$$

We obtain

$$\Phi(t) = \Phi_0 + \dot{\Phi}_0(t-t_0) - aC_1(t) - b\,C_2(t) + c\,C_3(t) + d\,C_4(t) + e\,C_5(t), \quad t > t_0. \tag{4}$$

Equation (4) is a model based on the force decomposition proposed in Eq. (2), the integrals needed to define the functions $F(t), I(t), J(t)$, and $C_i(t)$ can be computed using data from the HPC simulations carried out in Ref. [5]. To this end, n points $\tilde{\Phi}_k$, corresponding to times $t_k = h, 2h, ..., nh$, for $k \in 0, 1, 2, ..., n$ from the numerical simulations were chosen. The number of selected points was varied but was approximately 70 points per oscillation cycle in all cases.

With the values $\tilde{\Phi}_k$, the frequency ω_y and the functions $C_i(t)$ from Eq. (4) were calculated, and in this way, an approximation for $\Phi(t)$ based on the model proposed is obtained. The error at each selected point t_k can be calculated as the difference $E_k = \tilde{\Phi}_k - \Phi(t_k)$, which can be interpreted as a function of the parameters a, b, c, d, e. Defining $C_0(t_k) = \tilde{\Phi}_k - \Phi_0 - \dot{\Phi}_0(t_k - t_0)$ the error at each point is

$$E_k(a,b,c,d,e) = C_0(t_k) + a\,C_1(t_k) + b\,C_2(t_k) - c\,C_3(t_k) - d\,C_4(t_k) - e\,C_5(t_k),$$

and the sum of squared errors is

$$E(a,b,c,d,e) = \sum_{k=1}^{n} \left(E_k(a,b,c,d,e)\right)^2. \tag{5}$$

At this stage, the least squares method can be employed to obtain the parameters that minimize the previous equation, transforming the inverse problem into an algebraic system of equations that can be solved numerically.

3. Results

Estimates of the physical parameters are recorded in Table I and plotted as a function of the reduced velocity $u_r = 2\pi/\omega_0$ in Fig. 3. It can be observed that the added mass parameter decreases monotonically as the reduced velocity increases. Additionally, the force coefficient c_d has a maximum between $u_r = 3$ and $u_r = 5$ coinciding with the region of maximum oscillation amplitudes that occur in the upper branch. Furthermore, as expected, the constant term C_y is close to zero, since in the y direction the cylinder oscillates around $y = 0$.

To assess the effectiveness of the parameters identifier, Eq. (2) is solved using a fourth-order Runge-Kutta method with the parameters listed in Table I. The solution is compared to the HPC simulations from [5]. Figure 4 shows the comparison for the case $u_r = 7$. It can be observed that the model with the estimated parameters accurately reproduces the oscillations observed in the FSI HPC simulations.

This means that the model given by Eq. (2) is equivalent to the original VIV configuration, resulting in an estimation for the added mass parameter. Other values of u_r follow similar trends.

It is also noted that the resulting parameters are of the same order of magnitude as those predicted by the potential flow theory for cylinders in ideal fluid flow. This point is significant because, as is well known, inverse problems can

TABLE I. Estimated parameters in the y^* direction.

u_r	m_a	c_d	A_y	B_y	C_y
3.4	2.276288	-0.040848	0.000643	-0.000940	0.000250
4	1.743349	0.726861	-0.014885	0.057982	-0.000136
5	0.913285	0.255111	-0.005992	-0.022085	-0.000269
6	0.812994	0.045761	0.003157	-0.003236	3.02×10^{-5}
7	0.570051	0.061857	-0.000344	0.004169	0.000207
8	0.437175	0.011848	-0.000164	0.001019	0.000377
9	0.351795	0.050827	-0.000963	0.001963	0.000331

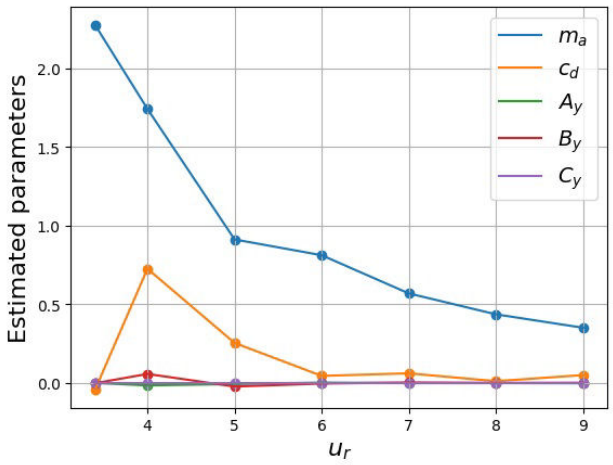

FIGURE 3. Graph of the parameters found in the y^* direction.

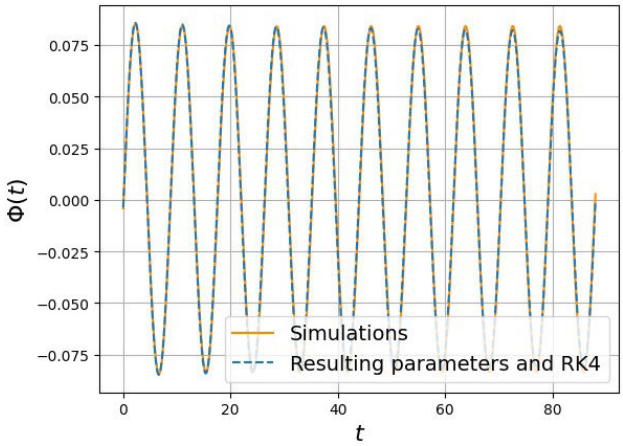

FIGURE 4. Comparison for $u_r = 7$ in y^* direction.

lead to over-determined algebraic situations where multiple solutions exist. Therefore, it is crucial to consider theoretical results that can help to distinguish between possible solutions.

3.1. Added mass as a function of angular acceleration

Now that we have a reliable approximation for the parameters representing the various contributions of the hydrodynamic force, we propose a function that approximately describes how the added mass parameter relates to the body's acceleration. It is anticipated that as acceleration increases, the effect of the added mass also increases. A representative value of the angular acceleration for each u_r case is calculated using the root mean square (RMS) value of the time history of the corresponding angular acceleration $\ddot{\Phi}(t)$.

A quadratic fit using the least squares method was performed, obtaining a mean square error $MSE = 0.064$. Considering the accuracy and the simplicity of this fit, the function proposed to describe the relationship between the added mass parameter and the angular acceleration is presented below, with its graph illustrated in Fig. 5.

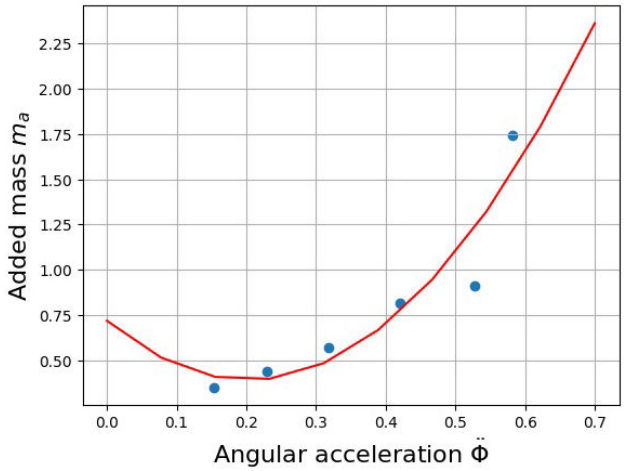

FIGURE 5. Adjustment for added mass m_a in the y^* direction.

$$m_a(\ddot{\Phi}) = 0.71815151 - 3.23594105\ddot{\Phi} + 7.98034256\ddot{\Phi}^2. \quad (6)$$

With the function given by Eq. (6), we can approximate the added mass parameter by knowing the angular acceleration of the cylinder. It is important to note that Eq. (6) was obtained from an inverse problem related to the damped forced oscillator equation, which can model a broad spectrum of VIV scenarios and even more general FSI problems. Additionally, it can be used to model the local behavior of small sections of deformable bodies. This leads the authors to think that Eq. (6) (or a variation of it) can assist in determining the added mass parameter for numerous applications.

4. Conclusions

Thanks to the interpretation of the hydrodynamic forces on the pivoted cylinder presented in Eq. (2), it became possible to propose and solve an inverse problem to estimate the added mass, the drag coefficient, and the forces driving the movement of a pivoted cylinder undergoing vortex induced vibrations. This resulted in a deeper understanding of the fluid-structure interaction inherent in this system. A quadratic function linking the added mass parameter to the angular acceleration of the cylinder was derived in Eq. (6). Through applied mathematics, a more precise comprehension of this system was attained.

The methodology followed in the present article is highly valuable, allowing for the analysis of other similar VIV cases through this inverse problem technique. Important design parameters can be identified if numerical or experimental data are available. Moreover, since turbulence is more common than not in real-life applications, it is noted that turbulent cases can be addressed similarly, provided a sufficient number of forcing frequencies are included in the hydrodynamic force decomposition in Eq. (2).

Finally, the relationship between the added mass parameter value and the angular acceleration given in Eq. (6) holds significant potential to improve the performance of general FSI simulations in the partitioned scheme. Flexible body sections can be viewed as collections of damped forced oscillators, allowing for the computation of local angular accelerations, and the ratio of the added mass parameter to the forcing amplitude can be estimated. With this information, an appropriate local under-relaxation factor would be readily available. Future work in this area is anticipated.

Acknowledgments

The authors acknowledge the financial support of the 'Consejo Nacional de Humanidades, Ciencias y Tecnologías' CONHACyT Mexico, through the project CONHACyT-CF21088.

1. Yuri Bazilevs, Kenji Takizawa, and Tayfun E. Tezduyar. Front Matter, in Computational Fluid-Structure Interaction: Methods and Applications. John Wiley & Sons, Ltd, (Chichester, UK, 2013). https://dx.doi.org/10.1002/9781118483565.fmatter
2. P. W. Bearman. Circular cylinder wakes and vortex-induced vibrations. *Journal of Fluids and Structures*, **27** (2011) 648, https://dx.doi.org/10.1016/j.jfluidstructs.2011.03.021.
3. Rémi Bourguet. Two-degree-of-freedom flow-induced vibrations of a rotating cylinder. *Journal of Fluid Mechanics*, (2020) https://dx.doi.org/10.1017/jfm.2020.403
4. J. C. Cajas, G. Houzeaux, M. Vázquez, M. García, E. Casoni, H. Calmet, A. Artigues, R. Borrell, O. Lehmkuhl, D. Pastrana, D. J. Yáñez, R. Pons, and J. Martorell. Fluid-structure interaction based on hpc multicode coupling. *SIAM Journal on Scientific Computing*, **40** (2018) https://dx.doi.org/10.1137/17M1138868
5. J. C. Cajas, D. Pastrana, I. Rodríguez, O. Lehmkuhl, G. Houzeaux, M. Vázquez, and C. Treviño. Vortex induced vibrations of a pivoted finite height cylinder at low reynolds number. *Physics of Fluids*, **33** (2021) 063602, https://dx.doi.org/10.1063/5.0051689
6. J. C. Cajas, I. Rodríguez, E. Salcedo, O. Lehmkuhl, G. Houzeaux, and C. Treviño. Aspect ratio influence on the vortex induced vibrations of a pivoted finite height cylinder at low reynolds number. *Physics of Fluids*, **35** (2023) 0164452, https://dx.doi.org/10.1063/5.0164452
7. W. Dettmer and D. Perić. A computational framework for fluid-structure interaction: Finite element formulation and applications. *Computer methods in applied mechanics and engineering*, **195** (2006) 5754,
8. Simon Gsell, Rémi Bourguet, and Marianna Braza. Two-degree-of-freedom vortex-induced vibrations of a circular cylinder at Re=3900. *Journal of Fluids and Structures*, **67** (2016) 156,
9. N. Jauvtis and C. H. K. Williamson. The effect of two degrees of freedom on vortex-induced vibration at low mass and damping. *Journal of Fluid Mechanics*, **509** (2004) 23.
10. A. Khalak and C. H. K. Williamson. Fluid forces and dynamics of a hydroelastic structure with very low mass and damping. *Journal of Fluids and Structures*, **11** (1997) 973, https://dx.doi.org/10.1006/jfls.1997.0110.
11. David Lo Jacono, Rémi Bourguet, Mark C. Thompson, and Justin S. Leontini. Three-dimensional mode selection of the flow past a rotating and inline oscillating cylinder. *Journal of Fluid Mechanics*, **855** (2018) 1, https://dx.doi.org/10.1017/jfm.2018.700
12. Miriam Mehl, Benjamin Uekermann, Hester Bijl, David Blom, Bernhard Gatzhammer, and Alexander Van Zuijlen. Parallel coupling numerics for partitioned fluid-structure interaction simulations. *Computers and Mathematics with Applications*, **71** (2016) 025, https://dx.doi.org/10.1016/j.camwa.2015.12.025
13. P. Moireau, N. Xiao, M. Astorino, C. A. Figueroa, D. Chapelle, C. A. Taylor, and J. F. Gerbeau. External tissue support and fluid-structure simulation in blood flows. *Biomech. Model. Mechanobiol.* **11** (2012)) 1,
14. D. Pastrana, J. C. Cajas, O. Lehmkuhl, I. Rodríguez, and G. Houzeaux. Large-eddy simulations of the vortex-induced vibration of a low mass ratio two-degree-of-freedom circular cylinder at subcritical reynolds numbers. *Computers Fluids*, **173** (2018) 118, https://dx.doi.org/10.1016/j.compfluid.2018.03.016.
15. Thomas Richter. Fluid-structure Interactions, volume 118 of Lecture Notes in Computational Science and Engineering. Springer International Publishing, (2017). https://dx.doi.org/10.1007/978-3-319-63970-3
16. E. Salcedo, C. Treviño, R. O. Vargas, and L. Martínez-Suástegui. Stereoscopic particle image velocimetry measurements of the three-dimensional flow field of a descending autorotating mahogany seed (swietenia macrophylla). *Journal of Experimental Biology*, **216** (2013) 085407. https://dx.doi.org/10.1242/jeb.085407
17. A. Santiago *et al*., Fully coupled fluid-electro-mechanical model of the human heart for supercomputers. *International journal for numerical methods in biomedical engineering*, **34** (2018) e3140,
18. T. Sarpkaya. A critical review of the intrinsic nature of vortex-induced vibrations. *Journal of Fluids and Structures*, **19** (2004) 389, https://dx.doi.org/10.1016/j.jfluidstructs.2004.02.005
19. C. H. K. Williamson and R. Govardhan, A brief review of recent results in vortexinduced vibrations. *Journal of Wind Engineering and Industrial Aerodynamics*, **96** (2008) 713, https://dx.doi.org/10.1016/j.jweia.2007.06.019

20. S. Wang, B. C. Khoo, G. R. Liu, and G. X. Xu, An arbitrary lagrangian-eulerian gradient smoothing method (gsm/ale) for interaction of fluid and a moving rigid body. *Computers fluids*, **71** (2013) 327,.

21. A. G. Malan and O. F. Oxtoby, An accelerated, fully-couple, parallel 3d hybrid finite-volume fluid-structure-interaction scheme. *Computational methods in applied mechanics and engineering*, **253** (2013) 426,

22. P. Causin, J. F. Gerbeau, and F. Nobile, Added-mass effect in the design of partitioned algorithms for fluid-structure problems. Computer Methods in applied mechanics and engineering, **194** (2005) 4506,

23. Christiane Förster, Wolfgang A Wall, and Ekkehard Ramm, Artificial added mass instabilities in sequential staggered coupling of nonlinear structures and incompressible viscous flow. *Computer methods in applied mechanics and engineering*, **196** (2007) 1278.